Characteristics of slug flow with inertial effects in a rectangular microchannel

Yao Chaoqun [a,b], Zhao Yuchao [a], Ye Chunbo [a,b], Dang Minhui [a,b], Dong Zhengya [a,b], Chen Guangwen [a,*]

[a] Dalian National Laboratory for Clean Energy, Dalian Institute of Chemical Physics, Chinese Academy of Sciences, Dalian 116023, China
[b] University of Chinese Academy of Sciences, Beijing 100049, China

HIGHLIGHTS

- Detail characteristics of slug flow with inertial effects are investigated.
- The transition of bubble formation regime mainly depends on the liquid velocity.
- The inertia of the forming bubble would lead to a faster rupture process.
- The inertial effects greatly thicken the liquid film thickness.
- A leakage flow is proposed to explain the bubble velocities and slug length.

ARTICLE INFO

ABSTRACT

Slug flow behavior and characteristics have been studied in a rectangular microchannel with Y-junction. Two simple bubble shape models are proposed to calculate the film thickness, gas hold-up and the specific surface area. The results show a significant effect of inertia on the bubble generation process. The liquid film thickness was greatly thickened by the inertial effect. The main forces on the rupture of the gas bubbles present a shifting from pressure (squeezing regime) to shearing stress and dynamical pressure of the liquid (shearing regime). The transition was found to mainly depend on the liquid velocity. A strong leakage flow of the liquid film around the gas bubbles was suggested as the liquid slug lengths decreased instead when liquid velocity increased. This leakage flow is also the reason of the over-prediction of the bubble velocity based on the stagnant film hypothesis.

1. Introduction

Gas–liquid two-phase flow pattern is an important research area for the multiphase systems in the microreaction technology. Among the flow patterns (Triplett et al., 1999; Zhao et al., 2013), slug flow is easily obtainable for a large range of operating conditions, and characterized by sequences of a gas bubble and a liquid slug. The figuration of slug flow contains regular sized gas bubbles that are longer than the channel diameter or width. The gas bubbles are surrounded by a thin liquid film with the bubble area occupying almost the entire channel cross-section (Fries et al., 2008; Thulasidas et al., 1995). Low axial mass transfer or back mixing occurs between two adjacent liquid slugs. Moreover, both radial mass and heat transfer can be intensified by internal circulation in the single slugs (Günther et al., 2004; Thulasidas et al., 1997). These merits make slug flow an ideal regime for improving the reaction performance. Wide attention has been paid to the bubble formation process (Fu et al., 2009; Garstecki et al., 2006; Pohorecki and Kula, 2008; van Steijn et al., 2007), the gas bubble and the liquid slug length (Garstecki et al., 2006; Leclerc et al., 2010; Qian and Lawal, 2006; Sobieszuk et al., 2010), the liquid film thickness around bubbles (Fries et al., 2008; Han and Shikazono, 2009a; Thulasidas et al., 1995), the phase distribution (Choi et al., 2011; Kawahara et al., 2005; Saisorn and Wongwises, 2010), the pressure drop (Kreutzer et al., 2005a, 2005b; Yue et al., 2009), and the mass transfer (Sobieszuk et al., 2011; van Baten and Krishna, 2004; Vandu et al., 2005), etc. However, a full understanding of slug slow for optimizing the design of microreactor remains pendent.

The characteristics of gas bubbles and liquid slugs have a direct impact on the gas–liquid transport and multiphase reaction

(Sobieszuk et al., 2011; Vandu et al., 2005). Their lengths are mainly affected by the gas bubble generation process at the junction, which can be attributed to the competition among the surface tension, the pressure, the shear stress, and the inertia. At low capillary numbers (Ca) and neglecting inertia, Garstecki et al. (2006) proposed the squeezing regime, in which the breakup of the gas bubbles is chiefly driven by the buildup of pressure upstream of an emerging bubble. In this case, the gas bubble length is independent of the fluid properties, and only depends on the two-phase flow rate ratio and the inlet geometry (Garstecki et al., 2006; van Steijn et al., 2010). At high Ca, the shearing regime occurs, which is characterized by the gas bubble partly occupying the cross section of the channel (Guo and Chen, 2009; Yue et al., 2008). Under this regime, the shear stress and inertia play an important role in the pinch-off. Thus, the fluid properties would have an influence on the bubble lengths (Abadie et al., 2012; Guo and Chen, 2009; Qian and Lawal, 2006). The gas bubble lengths, as well as the gas hold-up, are also affected by the aspect ratio of channels as indicated by Choi et al. (2010).

The liquid film around gas bubbles is also of great importance for mass and heat transfer. The thickness of liquid film has mainly been studied in circular capillaries that it was considered as a function of the capillary number (Ca) (Aussillous and Quéré, 2000; Bretherton, 1961; Han and Shikazono, 2009b; Kreutzer et al., 2005b). More recently, attention has been paid to microchannels with other cross sections (Fries et al., 2008; Han and Shikazono, 2009a; Kolb and Cerro, 1991; Kuzmin et al., 2011; Thulasidas et al., 1995). The liquid film distribution in square capillaries is not cylindrically symmetric due to the corners, which differs from that of their circular counterparts. The gas bubble shape in the cross section is also non-axisymmetric as the corners is affected by larger viscous forces than the regions near the center of the walls (Kolb and Cerro, 1991). However, the gas bubble shape presents a shifting from non-axisymmetric to axisymmetric above a transitional value of Ca ($O(10^{-2})$) (Fries et al., 2008; Han and Shikazono, 2009a; Kolb and Cerro, 1991; Kuzmin et al., 2011; Thulasidas et al., 1995), as shown in Fig. 1(b) and (c). Kreutzer et al. (2005a) developed an empirical correlation for estimating the liquid film thickness in the corners of square channels. Their results show that even at extremely low Ca, the liquid film does not vanish in the corners. Research on rectangular channels was motivated by the interest in monolithic reactors and by the easy fabrication of rectangular cross sections with MEMS techniques, such as photolithography and etching techniques. Moreover, the slug flow in rectangular channels presents different behaviors (Choi et al., 2011; Hazel and Heil, 2002; Kuzmin et al., 2011). Hazel and Heil (2002) investigated the steady propagation of a semi-infinite bubble into rectangular channels. Their numerical results indicated that at a given Ca, an increase in the aspect ratio caused a decrease in the liquid film thickness in the planes of the shorter semi-axis. The gas bubble shape turned into ellipsoid as the liquid film thickness increases (Fig. 1(e)). Kuzmin et al. (2011) found similar results from the simulation of the slug flow in rectangular channels using lattice Boltzmann method.

In most of the literatures considering the liquid film thickness, Ca was varied by increasing the liquid viscosity, so the Reynolds number (Re) was always small (Kolb and Cerro, 1991; Thulasidas et al., 1995). Many results have shown that the inertia has a considerable influence on the liquid film thickness and the gas bubble shape (Aussillous and Quéré, 2000; Han and Shikazono, 2009a; Heil, 2001; Kreutzer et al., 2005b). For a given Ca, a decrease in the liquid film thickness up to Re of about 100, followed by an increase for higher Re was numerically discovered by Kreutzer et al. (2005b) and Heil (2001). Aussillous and Quéré (2000) reported the thickening effect of inertia with low viscosity fluid and proposed an inertia-dependent scaling law for qualitatively explaining this effect as $\delta/D_H \sim Ca^{2/3}/(1+Ca^{2/3}-We)$. Han and Shikazono (2009a) investigated the effect of inertia in square capillaries using different working fluids and developed a similar correlation, which showed good agreement with experimental data. In the present study, the thickening effect of inertia in the rectangular channel with an aspect ratio of 2.68 has been shown to be more obvious.

The present work aims at improving the fundamental understanding of slug flow in rectangular microchannel with inertia effect. Information about the gas bubble generation process, the length of the gas bubble and the liquid slug, the liquid film thickness, the gas bubble velocities, and the gas hold-up, will be investigated through visualization methods in a rectangular microchannel with Y-junction.

2. Experimental section

2.1. Microchannel specification

A rectangular microchannel contactor with Y shaped junction was used in this work. All the channels, with a cross section of 750 μm (width) and 280 μm (depth), were fabricated on polymethal methacrylate substrate (PMMA, A grade, 92% of light transmittance, ShenZhen HuiLi Acrylic Products Co., Ltd) using micromachining technology (FANUC KPC-30a) in our CNC Machining Center. The schematic representation and actual picture of the microchannel reactor construction are displayed in Fig. 2. The two PMMA plates were sandwiched between two stainless steel plates and sealed by screws. The angle between gas and liquid inlets is 60° and the length of the mixing channel is 60 mm.

2.2. Experimental setup

The experiments were mainly conducted with deionized water–carbon dioxide and a small number of experiments were by deionized water–nitrogen. The schematic diagram of the experimental setup was shown in Fig. 3. Gas flow was provided via the pressure regulator and controlled by mass flow controller (D07-7B, Beijing Sevenstar Electronics Co., Ltd., China) with an accuracy of 0.5% full scale. Deionized water was pumped by a high precision digital piston pump (Series II, Chrom. Tech. Inc.). The actual flow rate under each run was determined by weighing method. In order to eliminate the pulsation of the liquid flow rate, a buffer tank was introduced before the microreactor inlet. After
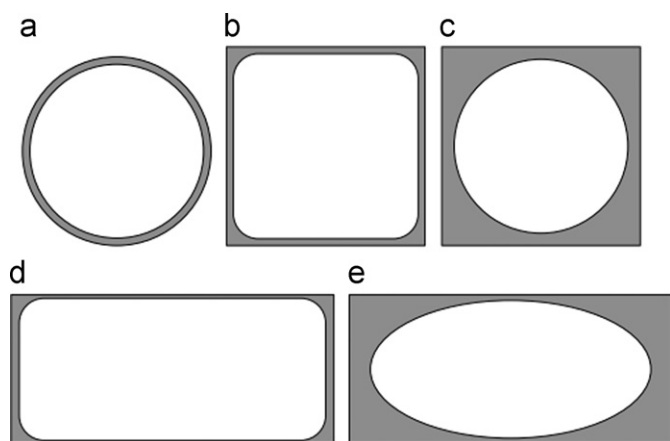

Fig. 1. Scheme of the liquid film distribution around gas bubbles in microchannel with different cross sections. (a) Circular channel, (b) square channel under transitional Ca, (c) square channel above transitional Ca, (d) and (e) rectangular channel.
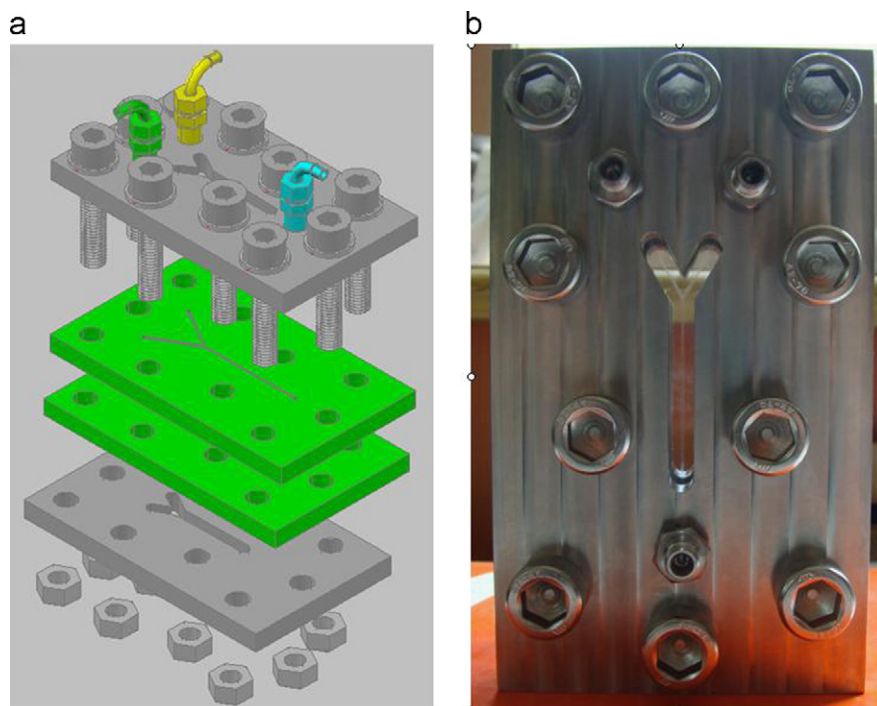
Fig. 2. (a) Construction of Y-junction microchannel reactor, (b) actual picture of construction of Y-junction microchannel reactor.
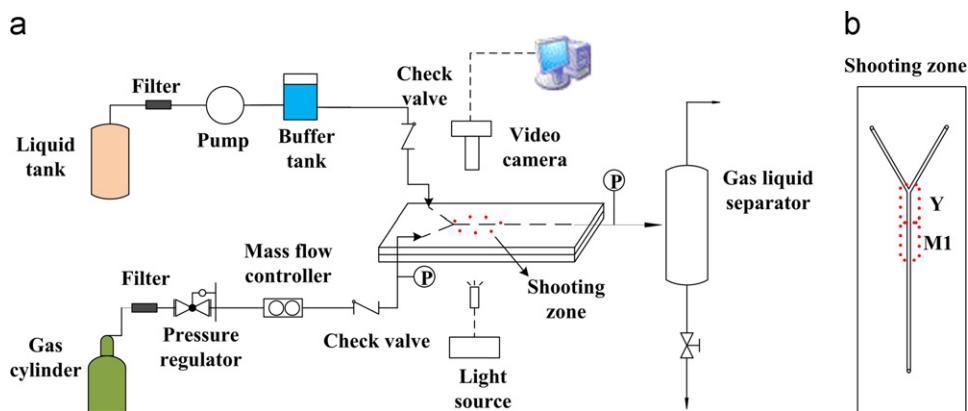

Fig. 3. Schematic of the experimental setup.

flowing through the microchannel contactor, gas and liquid were separated in a gas–liquid separator. The pressure drop was directly recorded by two pressure transducers inserted in the gas inlet and the outlet, respectively. All experiments were conducted under ambient conditions.

The pattern was recorded by a CMOS high-speed camera system (BASLER A504kc). The CMOS camera was placed above the visual window. For avoiding possible heating of the microchannel, a cold light source was placed beneath the visual window to provide strong light. In all experiments, the CMOS camera was set to work at a recording rate of 1000 frames/s and a resolution of 1280×512 pixels. The shutter time was adjusted between 40 and 80 µs. The region of interest includes the Y-junction and a zone covers a length from 10 to 23 mm downstream of the Y-junction, which is marked in Fig. 3(b) as Y and M1, respectively.

2.3. Image processing

The images acquired from M1 zone were used to analyze the gas bubble and the liquid slug lengths, as well as the gas bubble velocities. For the measurement of these characteristics, a Matlab-based program (Matlab R2009b) was developed to process the images. First, an image was converted to a binary array where locations associated with the gas bubbles and the liquid slugs (bright region) are assigned a value of '1' while locations associated with the gas–liquid interfaces (dark region) are assigned a value of '0'. After removing contaminants and filling holes, all the gas bubbles and the liquid slugs in each image can be detected, and then their locations (centroid location), the gas bubble length (L_B) and the liquid slug length (L_S) can be easily determined. The gas bubble travel distance, which is obtained from two successive images, is divided by the time interval (1 ms) to obtain the gas bubble velocities. Due to the lack of the knowledge of the liquid film thickness, some assumption and simplification were made to calculate the specific surface area (a) and the gas hold-up (ε). This will be discussed in the following sections. Under each operational condition, a sequence of at least 100 images, which corresponded to 200 to 1000 bubbles, was analyzed and the data were averaged to obtain the final value. The relative standard deviation (RSD) of the bubble and slug length did not exceed 4.3%.

3. Results and discussion

3.1. Bubble formation

3.1.1. Bubble formation

Fig. 4 shows the two kinds of gas bubble generation mechanisms in the Y-junction. The squeezing regime was found at lower liquid velocities. It can be divided into two stages, the filling stage where the bubble fills the entire channel width, and the squeezing stage where the bubble neck contracts until pinch-off (Fig. 4a). It is notable that very long bubbles are formed at large gas–liquid flow rate ratio which may result in a relatively strong deviation in the gas bubble length. When the shear stress begins to play an important role in the break process, the shearing regime would be expected. Typical images of the shearing regime were demonstrated in Fig. 4(b) and (c). It is obvious that the emerging gas bubble only partly blocks the microchannel. Also shown in Fig. 4 is that for the squeezing regime the gas liquid interface ruptures far from the Y-junction while much closer to the Y-junction for the shearing regime. Commonly, the gas bubble ruptures right at the gas–liquid intersection (Garstecki et al., 2006; Guo and Chen, 2009) while at downstream of the intersection (Guo and Chen, 2009). The different observation here was mainly due to the Y-type structure. The gas thread was under the impingement of the liquid inertia or dynamical pressure. As the liquid velocity increased, the rupture point moved closer to the Y-junction. The transition from the squeezing to the shearing regime was found to be mainly influenced by the liquid velocity as shown in Fig. 5, which was also observed by Yue et al. (2008). However, an earlier transition happened at 0.2 m/s (j_L) compared to their results. This may result from a much higher aspect ratio of the microchannel used in this work.

The gas bubble formation period was estimated simply by recording the time interval between two successive gas bubbles. The dependency of the gas bubble formation frequency (f) on the gas and liquid velocities is displayed in Fig. 6. As can be seen, f increases with increase in the liquid velocity. This can be explained by the fact that the component of liquid dynamical pressure normal to the main channel and the shear stress exerted on the gas bubble tip both increase at higher liquid flow rates. As to the gas velocity, the effect is less obvious. It is harder for the gas–liquid interface to rupture at larger gas velocity. However, a larger gas velocity leads to a higher inertia of the emerging bubble, which speeds up the rupture process. These two antagonistical effects make f only slightly increase with gas velocity. At constant liquid velocity, there is an asymptotic value for further increasing gas velocity as also observed by Arias et al. (2009). It was explained by the existence of a limiting scale for bubble generation process, which is the time needed by the liquid flow to cross a distance of

the order of the capillary size (Arias et al., 2009). The bubble formation frequency *versus* the gas–liquid flow rate ratio is also plotted in Fig. 6(b). For a given j_G/j_L, f increases with the gas velocity since the liquid velocity increases simultaneously.

3.1.2. Bubble and slug lengths

Fig. 7 shows the evolution of the gas bubble and the liquid slug lengths as a function of the gas–liquid flow rate ratio at different gas superficial velocities. For a given flow rate ratio, the bubble and slug lengths both decrease when the two-phase superficial velocity increases. This decrease in bubble and slug size can be explained by the increase in energy input to the system (Abadie et al., 2012). Thus, the frequency of the bubble formation greatly augmented with inertia as shown in Fig. 6. It should be noted that the dimensionless bubble lengths larger than 9 at high flow rate ratios were not displayed as less bubbles were captured by the camera and deviation in length became relatively larger.

Garstecki et al. (2006) proposed a simple model which linearly scales with the gas–liquid flow rate ratio for the estimation of bubble lengths. It was developed based on their work conducted in microchannel at low Ca (<0.01) and Re (<1). van Steijn et al., (2007, 2010) improved the model by taking a leakage flow around the forming bubble in rectangular channels and the inlet geometry into account as:

$$\frac{L_B}{W} = \lambda_1 + \lambda_2 \frac{j_G}{j_L} \tag{1}$$

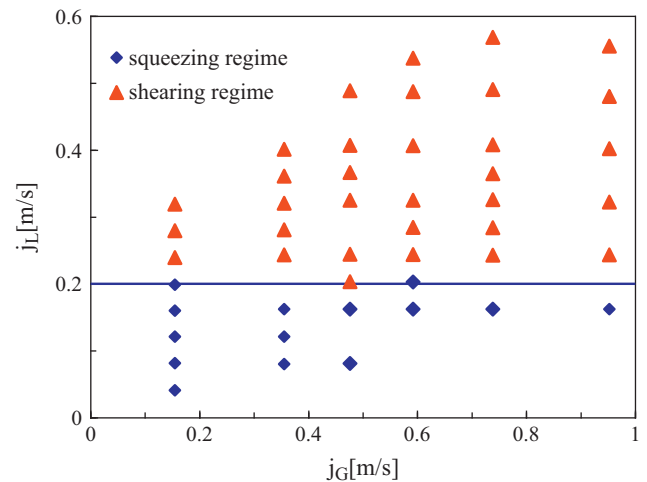This form originates from the so-called "squeezing regime", under which the bubble formation is mainly dominated by

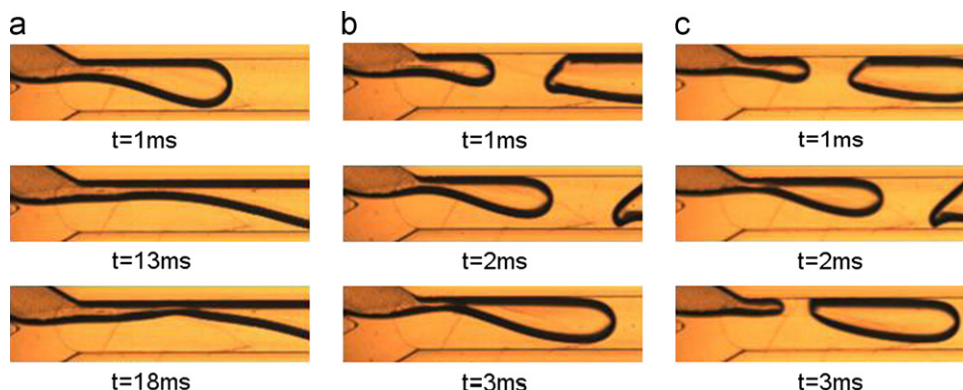**Fig. 5.** Transition from squeezing pattern to shearing pattern.

Fig. 4. Bubble formation in Y-junction in CO_2–H_2O system. (a) j_G=0.356m/s, j_L=0.081m/s, We=1.05, Ca=0.0059, (b) j_G=0.476m/s, j_L=0.325m/s, We=3.53, Ca=0.0108 and (c) j_G=0.592m/s, j_L=0.407m/s, We=5.48, Ca=0.0135.
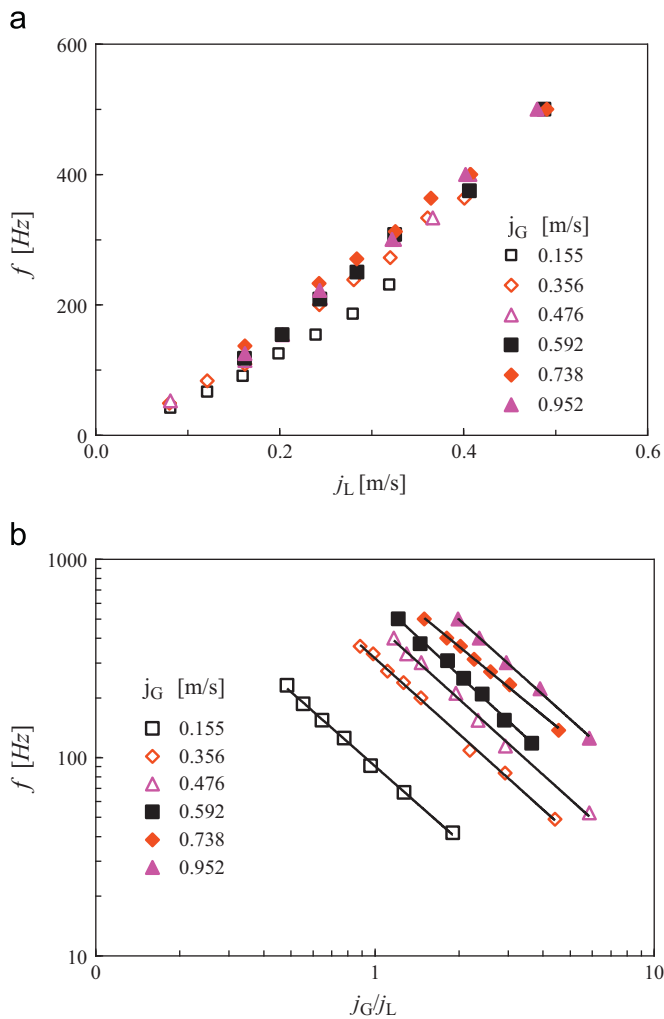
Fig. 6. Frequencies of bubble formation.

Fig. 7. (a) Dimensionless bubble length and (b) dimensionless slug length *versus* gas liquid flow rate ratio for varying gas phase velocities.

pressure difference across the forming bubble as the effects of shear stress and inertia are negligible compared to the pressure difference. λ_1 refers to the bubble growth in the filling stage and λ_2 refers to the interface shrinking in the squeezing stage.

It can be seen in Fig. 7(a) that for a constant gas velocity, the linear evolution agrees well with the above relationship whereas the slop λ_2 decreases as the gas superficial velocity increases. This implies the squeezing mechanism no longer applies to the gas bubble formation process here as the shear stress and inertia effect play significant roles. According to Garstecki et al. (2006), the bubble size is determined by the squeezing time $d_{neck}/u_{squeeze}$. The slope λ_2 stems from the scaling relation $(d_{neck}/u_{squeeze})/W \times u_{growth} \sim d_{neck}/W \times (Q_G/Q_L) \sim \lambda_2 \frac{j_G}{j_l}$. As stated before, the inertia of the emerging gas bubble would speed up the rupture process. Then the decrease in the slope λ_2 could be explained by that the contribution of the inertia is reflected in a larger '$u_{squeeze}$' and thus a smaller λ_2. The larger slope at $j_G=0.952$ m/s may be caused by a strong shrinkage of bubble area in the cross section of the microchannel. The shrinkage of bubbles at large gas velocities is shown in Fig. 11.

The dimensionless liquid slug length as a function of j_G/j_L is displayed in Fig. 7(b). The slug length increases with increase in j_G/j_L for a given gas velocity, implying a negative relation between the slug length and liquid velocity. The result presents a different behavior compared to literatures (Abadie et al., 2012; Hui Liu and Rajamani, 2005; Laborie et al., 1999; Leclerc et al., 2010; Qian and Lawal, 2006; Völkel, 2009). Leclerc et al. (2010) reported that the
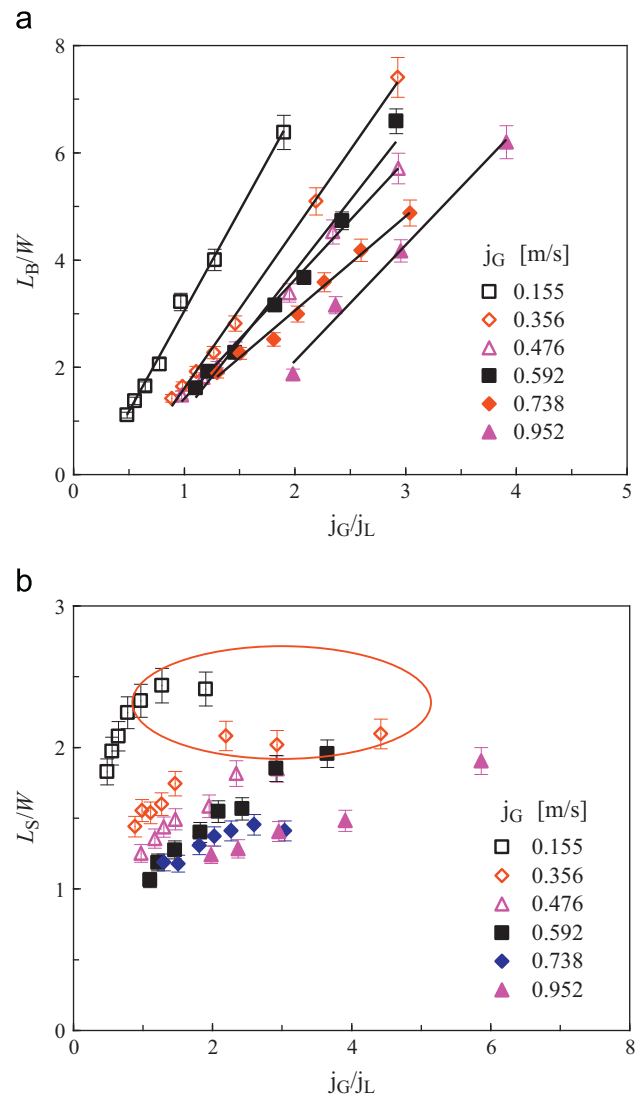
slug length first decreased rapidly and then kept nearly constant for increasing Q_G/Q_L in a square microchannel. Results from Akbar and Ghiaasiaan (2006), Hui Liu (2005), Qian and Lawal (2006) showed a positive relation between liquid velocity and slug length. Abadie et al. (2012) and Völkel (2009) reported that slug lengths in rectangular microchannels decreased with increase in j_G/j_L. Only parts of Kreutzer et al. (2005c) results included a decline as liquid hold up increased when the hold up was smaller than 0.3. Clearly, the situation about liquid slug length is more complex than the bubble length, for which the tendency is generally clear and unanimous. To explore the relationship between the slug length and the liquid velocity, the mechanism of the slug formation should be studied.

Pohorecki and Kula (2008) proposed a 'switching' mechanism to predict the gas bubble and liquid slug lengths in Y-junction. In this context the estimate of slug length is based on the assumption that the slugs and bubbles form alternately that the time for each phase to break up is equal to the time the other phase needs to fill the entire channel cross section. Then the slug length should scale as α_G^{-1}. Völkel (2009) suggested that liquid slug length should scale as j_L/j_G, which agrees with their data and Abadie et al. (2012). As the two analyses have certain theoretical basis, the decrease in slug length as liquid velocity increases may originate from the

leakage flow in the corners (Harris Wong and Morris, 1995; Kolb and Cerro, 1993; Völkel, 2009; van Steijn et al., 2007). The amount of liquid in a slug would reduce even though the liquid flow rate increases as long as the leakage is stronger. This leakage flow scales as $Ca^{-1/3}$ and could be comparable to the bubble velocity under certain conditions according to the numerical results of Harris Wong and Morris (1995). Unlike the small influence of the leakage flow in Völkel's (2009) work, the influence was much stronger as the flow rates used here were much more larger. Actually, liquid slug length stops increasing when the liquid flow rate is small, as specified by the red ellipse in Fig. 7(b), which means a less significant leakage.

To interpret the bubble lengths with inertia effect in the present study, a modification of the Gastecki model was proposed:

$$L_B/W = j_G/j_L + 1.37We^{-0.349}j_G/j_L \qquad (2)$$

The power of We is negative, indicating additional influence of inertia on bubble formation. The comparison of experimental data with predictions of Qian and Lawal (2006), Sobieszuk et al. (2010) and Eq. (2) is shown in Fig. 8(a). It should be noted that their data obtained from circular or square capillaries were normalised by the hydraulic diameter and compared to the dimensionless bubble length in this work. In that case, Sobieszuk's correlation agrees

better than Qian and Lawal's with our results. Experiments of another fluid pair of N_2–H_2O were conducted to test the validity of Eq. (2) and the fitting performance was good.

An empirical correlation for estimating the slug length was also developed as

$$L_S/W = 1.157\beta^{-0.365}(1-\beta)^{-0.373}We^{-0.208} \qquad (3)$$

where $\beta = j_G/(j_G + j_L)$, Eq. (3) shows good agreement with experimental results as shown in Fig. 8(b).

3.2. Film thickness

3.2.1. Bubble shape model

Many researches have focused on the gas bubble shape and the liquid film thickness in square capillaries or microchannels (Fries et al., 2008; Kolb and Cerro, 1991; Thulasidas et al., 1995). So far, experimentally determining film thickness and bubble shape in microchannels is rather difficult, especially with rectangular cross-section. In micro devices, the most often used technique to characterize gas–liquid flow is flow imaging with high speed camera. A typical flow pattern of slug flow captured by high speed camera is shown in Fig. 9(b); sequences of a gas bubble and a liquid slug flow through the microchannel. The darker region is caused by the strong light reflection of gas–liquid interface, which is represented as red lines in Fig. 9(a). The darker line around the bubbles is also due to the curvature of the G–L interface. The rectangular microchannel used in this work has a large aspect ratio of 2.68, which is larger than the critical value of 2.04, above which the transition from nonaxisymmetric to axisymmetric bubble never happens at any Ca (Hazel and Heil, 2002). The cross section of the gas bubbles in this work was always nonaxisymmetric under all experimental conditions. It could be deduced from images that the width of bright areas inner bubbles (Fig. 9(b)) was always larger than the depth of the microchannel. Based on these facts, two simple models of bubble shape as shown in Fig. 9 (a) were assumed to calculate film thickness in the corners and bubble volume, which leads to the determination of gas hold-up in microchannels. Model 1 assumes that the interface at the corner is a quadrant and the quadrants are connected by a straight line while model 2 assumes that the gas–liquid interface is arc-shaped. Model 1 is suitable for the conditions of low liquid and gas velocities when the film thickness is thin while model 2 is suitable for the conditions of thick film at high liquid and gas velocities as surface tension restores the arc shape due to reduced wall
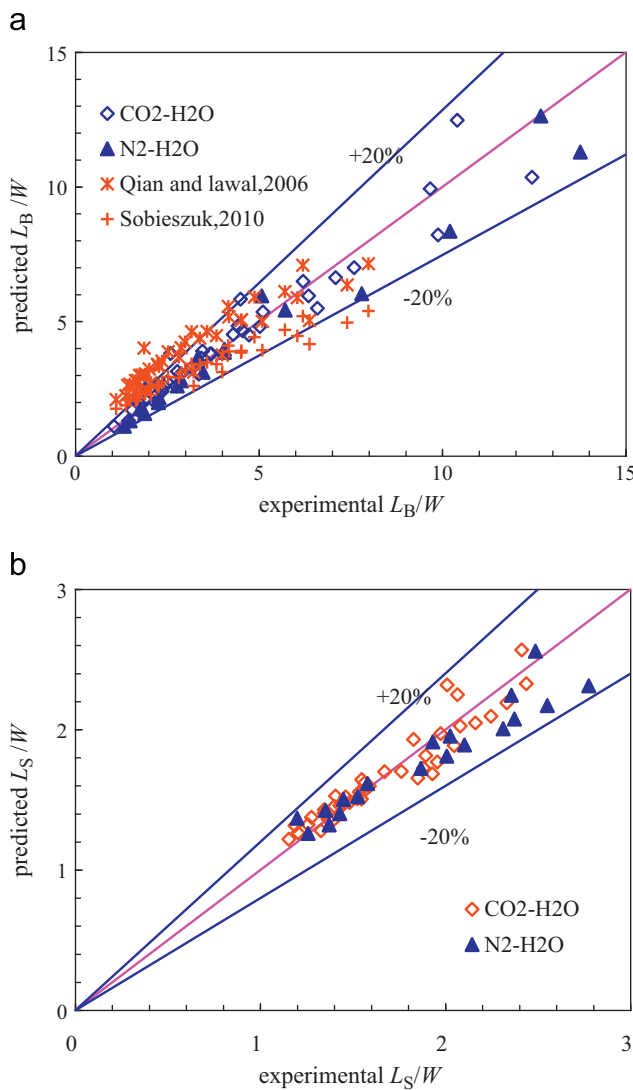

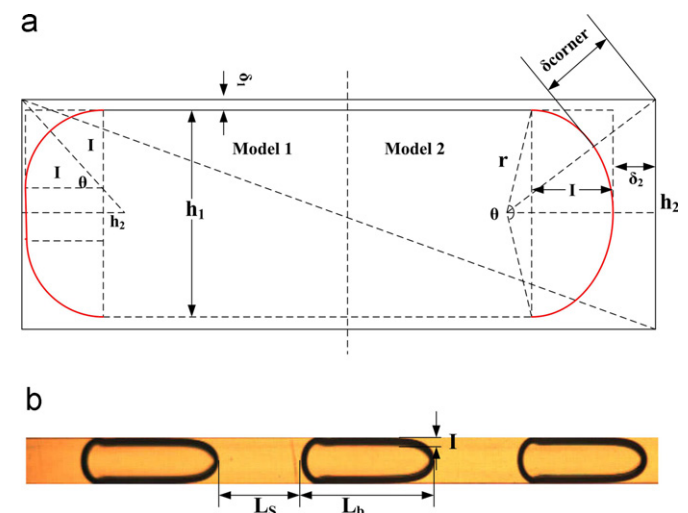**Fig. 8.** Predictions of (a) bubble length and (b) slug length *versus* experimental values.

Fig. 9. (a) Schematic representation of the cross-sectional bubble shape and liquid film distribution (b) typical slug flow pattern.

confinement. However, when both models were applied to calculate film thickness in the corners, specific surface area and gas hold-up, the deviation was rather small. The bubble caps were treated as spherical caps to calculate the specific surface and the gas hold-up.

3.2.2. Film thickness

The thickness of film around bubbles in capillaries with circular cross-section is a function of the capillary number Ca (Bretherton, 1961). Kolb and Cerro (1991) extended this work to square capillaries and indicated that when Ca was less than 0.1, the bubble is non-axisymmetric. This transitional value of Ca was later revised to 0.04 by Thulasidas et al. (1995). Under this condition, the film thickness in the planes varies very little and could be assumed to be $0.02D_H$ (Fries et al., 2008; Kolb and Cerro, 1991). The research results mentioned above were conducted in circular or square capillaries and are not valid when inertia effects play a significant role.

The superficial velocities we chose ranged from 0.02 to 0.95 m/s for the gas and 0.04 to 0.57 m/s for the liquid. Under the experimental conditions, the Ca varies from 0.002 to 0.02, while the We varies from 0.21 to 12.5 (corresponding relationship shown in Fig. 10). In this case, the inertial effect cannot be neglected. It was observed in our experiments that when We exceeded a value about 3.1, the darker region of bubbles were stripped off from the channel walls, which meant that the film thickness increased greatly. When these conditions occurred, film thickness at side walls δ_2 could be approximated by counting the pixels between the channel wall and gas–liquid interface. This phenomenon was shown in Fig. 11. As can

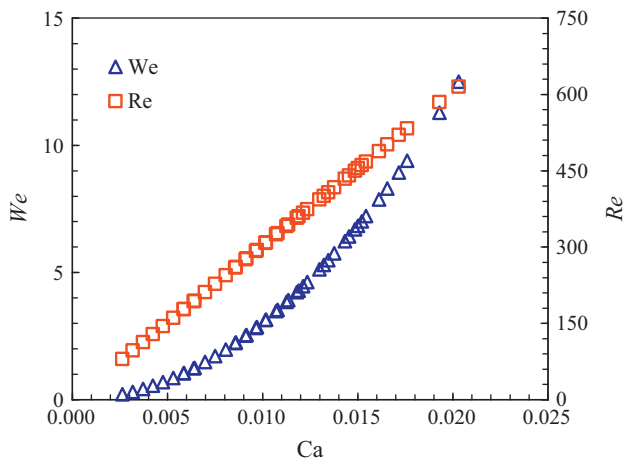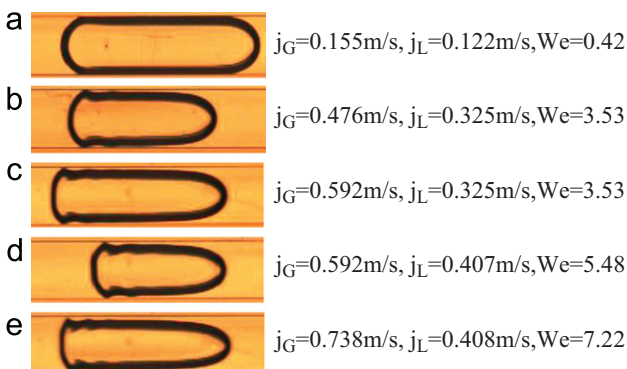be seen, the film thickness increases when either gas or liquid velocity increases. Increasing the We also changes the bubble shape. At low velocity conditions, both the bubble caps at the leading nose and the rear end are symmetric and controlled by the surface tension. At higher velocities, the bubble nose becomes more sharpened and the bubble rear more flattened. The whole bubble looks more like a bullet due to inertia effect.

Based on the discussion above, when calculating the film thickness in the corners, film thickness δ_2 at side walls was set as $0.02D_H$ at low We values (less than 3.1), and calculated directly from images at large We values. Data of the film thickness, the gas hold-up and the specific surface area presented in this paper for analysis were obtained using model 1 in the first case and using model 2 in the second case. At all conditions, film thickness δ_1 at top and bottom planes was set as $0.02D_H$.

Results of the film thickness are plotted against Ca, together with correlations from literature, in Fig. 12. Film thickness at the corner is well predicted by correlation given by Han and Shikazono (2009a) and Kreutzer et al. (2005a) at low Ca (< 0.01). Under this regime, the liquid film thickness increases slightly as Ca increases. A little over-prediction can be explained by rectangular microchannel used here. However, when Ca moves to a larger region, the Kreutzer correlation strongly underestimates the experimental data. Note that the Kreutzer correlation was obtained by mathematical fitting data from Hazel and Heil (2002), Kolb and Cerro (1991), Kreutzer et al. (2005a), Thulasidas et al. (1995) for square capillaries. The upper limit ($Ca \rightarrow 0$, $Ca < 0.01$) was based on the data of Thulasidas et al. (1995) alone with working fluid of water and air. The rest of the data were all silicone oil of high viscosity (Kolb and Cerro, 1991; Thulasidas et al., 1995) or simulation results from Hazel and Heil (2002). These results all excluded significant effect of inertia, which could be the explanation for the poor prediction at high Ca values. The correlation from Han and Shikazono (2009a) embodies the effect of inertia by introducing We as proposed by Aussillous and Quéré (2000). At relatively low Ca with small inertia, the correlation agrees well with Kreutzer et al. (2005a). As the Ca increases, the film thickness shows larger increase due to the inertia effect. The film thickness in the corners could be as large as 124.4 μm. The thickening effect of inertia in this work was much larger than in the work of Han and Shikazono (2009a). It may be ascribed to the rectangular cross-section as Hazel and Heil (2002) showed that the fluid was driven from the horizontal planes towards the vertical planes.

The liquid film thickness at side walls were displayed only when bubble detachment occurred, that was when We was larger than 3.1. Large deviation from literature was also observed.

Fig. 10. Weber, Reynolds and capillary numbers of the experiments.

a — j_G=0.155m/s, j_L=0.122m/s, We=0.42

b — j_G=0.476m/s, j_L=0.325m/s, We=3.53

c — j_G=0.592m/s, j_L=0.325m/s, We=3.53

d — j_G=0.592m/s, j_L=0.407m/s, We=5.48

e — j_G=0.738m/s, j_L=0.408m/s, We=7.22

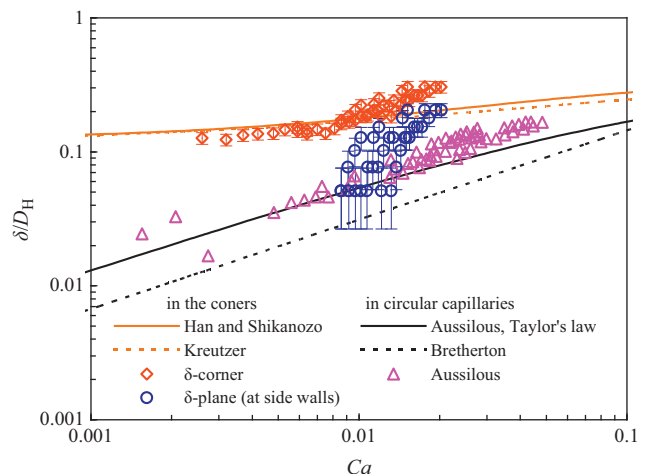**Fig. 11.** Bubble shapes and bubble detachment with inertia effect.

Fig. 12. Film thickness against capillary number.

The liquid film thickness data scatter very much. This is due to the different contribution of liquid and gas velocities to the film thickening effect. As shown in Fig. 11, the film thickening can be directly observed as gas velocity or liquid velocity increases. The model by Bretherton (1961) and the Taylor's law (Aussillous and Quéré, 2000) both scale with $Ca^{2/3}$ for visco-capillary regime in circular capillaries. Under visco-capillary regime, the gas–liquid interface was governed by capillary forces and surface tension while the inertia effect was neglected. The inertia effect on the film thickness here was also much stronger than that in circular capillaries (Aussillous and Quéré, 2000), as shown by triangular symbols in Fig. 12.

Since inertia and geometry play important roles in gas–liquid flow in rectangular microchannels, these results are reasonable. Many simulation results have indicated that under slug flow, wall pressure increases drastically when a bubble passes through (Abadie et al., 2012; Kreutzer et al., 2005a). In square tubes, the fluid particles tend to move towards the corners, which offer less resistance to the flow than the thinner regions along the walls of the tube (Hazel and Heil, 2002). As to the rectangular microchannel with large aspect ratio, the tendency is more obvious. The gas and liquid continuously flow into the microchannel continuously through a Y-junction in the present study. Increasing the superficial velocity of gas or liquid would both have an influence on flow behavior and the liquid film thickness. This kind of operating mode was different from the work by Aussillous and Quéré (2000) and Heil (2001), which involved semi-infinite bubble propagation process.

3.3. Bubble velocities

During slug flow, bubbles are surrounded by a thin film region, which isolates bubbles from the channel wall. The bubble velocities determine the residence time of the reaction material in the microchannel reactor. Bubbles generally move faster than the velocity of the liquid in the slug, which is usually expressed as two-phase superficial velocity for simplicity (Abiev, 2008). Applying volume continuity leads to the equation:

$$U_B A_B + U_{film} A_{film} = j_{TP} A_{mc} \tag{4}$$

Thus, the bubble velocity is derived as

$$U_B = \frac{A_{mc}}{A_B} j_{TP} - \frac{U_{film} A_{film}}{A_B} \tag{5}$$

If the velocity of the liquid film can be neglected, the bubble velocities should be linear with respect to the two-phase superficial velocity:

$$U_B = \frac{A_{mc}}{A_B} j_{TP} \tag{6}$$

Fig. 13 displays the measured U_B from images as a function of j_{TP} for the rectangular microchannel. It can be observed that the bubble moves faster than the liquid in the slug, which is more obvious at higher velocities. Also shown in Fig. 13 is the linear relationship between bubble velocity and the total superficial velocity as indicated by Eq. (6). This linear relationship was observed in many literatures (Abadie et al., 2012; Choi et al., 2010; Taha and Cui, 2004; Yue et al., 2009), which usually explained the relationship with stagnant film hypothesis that the liquid film velocity is negligible. The slope of the regression line (red line) was determined to be 1.12, which is comparable with Choi et al. (2010). However, it is only a mean value of the experimental conditions since A_{mc}/A_B did not keep constant. The bubble area decreases when the liquid film in the corner or at side walls thickens in cases gas and liquid velocity increase, as discussed in part 3.2.
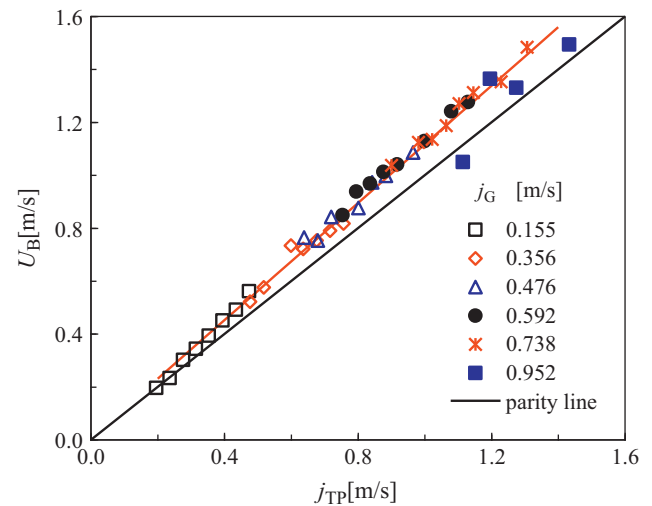

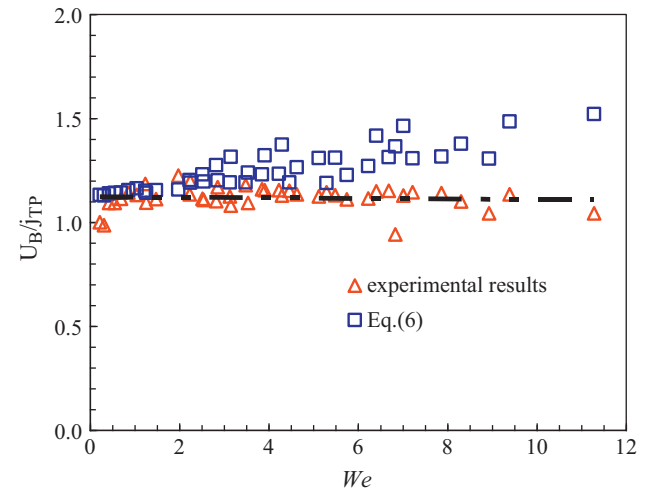Fig. 13. Bubble velocities *versus* two-phase velocity.

Fig. 14. Ratio of bubble velocity to liquid two-phase superficial velocity *versus We*.

Since the bubble shape models were proposed, the bubble area A_B and A_{mc}/A_B could also be calculated. With the assumption that the liquid film velocity was negligible, the bubble velocity was estimated from Eq. (6). The comparison between the estimated and determined velocities is plotted in Fig. 14. It can be seen that the experimental data agree well with the predictions of Eq. (6) at low *We* numbers. However, the predicted value deviates from the experimental bubble velocity at higher *We* numbers. This again implies that a relatively significant bypass flow exists in the corners (Harris Wong and Morris, 1995; Kolb and Cerro, 1993). With a large aspect ratio, the fluid is driven to the side walls and the corners for the larger flow resistance at the top and bottom walls with thinner film. Thus, when the liquid film around the bubble thickens at high *We* numbers, the bubble area in the cross-section reduces, which should lead to a higher A_{mc}/A_B at high velocities. A bypass flow could offset this augment in Eq. (6).

3.4. Gas hold-up and void fraction

The volumetric gas hold-up (ε) and void fraction (α) are important parameters in gas–liquid two phase flow as they are indicative of the flow regimes and heat or mass transfer. Also gas hold-up is usually used to evaluate accelerational terms in the total pressure drop of gas–liquid flow (Yue et al., 2008, 2009).
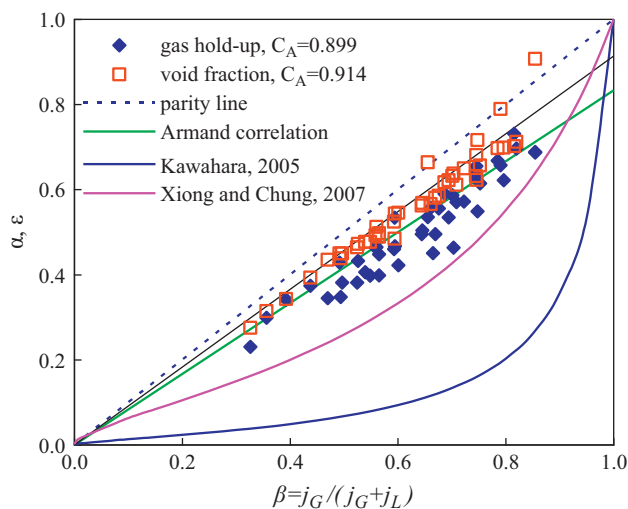
Fig. 15. Comparison of gas hold-up with literature.

Fig. 16. Specific surface area under different conditions.

There are already plenty of literature studies that consider void fraction in small/micro- capillaries or channels (Choi et al., 2011; Chung and Kawaji, 2004; Ide et al., 2007; Kawahara et al., 2009, 2011, 2005; Saisorn and Wongwises, 2009, 2010, 2011; Xiong and Chung, 2007; Yue et al., 2008). Generally, the void fraction correlation for microchannels as a function of volumetric quality (β) can be classified to two types: linear relationship of Armand-type $\alpha = C_A\beta$ and non-linear relationship of $\alpha = C_1\beta^{0.5}/(1-C_2\beta^{0.5})$. An interesting phenomenon arises when simply summarizing these reported results in microchannels with diameters less than 1.0 mm. It seems that the Armand-type correlation describes well the void fraction for circular capillaries when the inner diameter is larger than 0.2 mm, while the non-linear correlation describes well for smaller capillaries (Chung and Kawaji, 2004; Kawahara et al., 2005; Saisorn and Wongwises, 2010). In square microchannels, the situation is more complex as the experimental data is scarce and deviates from each other (Kawahara et al., 2011; Xiong and Chung, 2007; Yue et al., 2008). However, Xiong and Chung (2007) found a tendency from linear to non-linear correlation when channel size decreased, which is in accordance with circular capillaries. This implies a stronger velocity slip between two phases in smaller capillaries. In rectangular microchannels (Choi et al., 2011) the void fraction all correlates well with volumetric quality in Armand-type correlation but the size effect on the coefficient C_A is not clear. Their work showed a negative relationship between the coefficient C_A and aspect ratio instead of hydraulic diameter.

In this work, the void fraction was calculated using the simple relation Eq. (7) and the gas hold-up in the M1 zone was determined by calculating the total gas bubble volume with the bubble models.

$$\alpha = \frac{j_G}{U_B} \qquad (7)$$

The results and comparison with literature are displayed in Fig. 15. It can be seen that both the gas hold-up and the void fraction follow the Armand-type correlation. It is interesting that the gas hold-up and the void fraction agree reasonably well considering the experimental error and idealization of the models. The coefficient C_A was determined to be 0.914 and 0.899, respectively, which was in accordance with the results of Choi et al. (2011), with respect to the aspect ratio.

3.5. Specific surface area

One of the main advantages of microreactors is the significant intensification of the mass transfer with large specific surface area
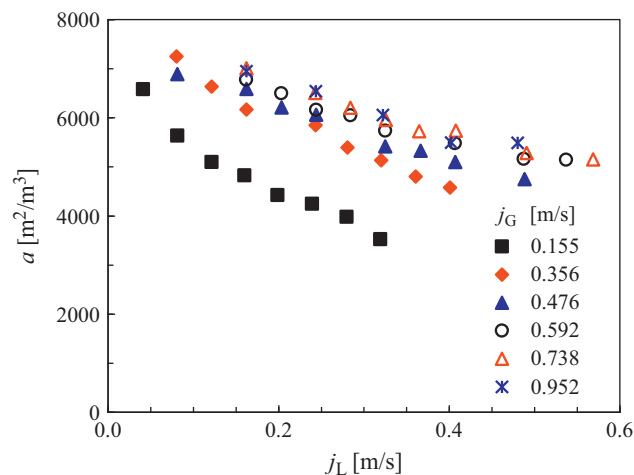
(Yue et al., 2007). As in conventional gas–liquid contactors, chemical and physical methods can be applied to determine the specific surface area in microreactors. When applying chemical methods, mainly with fast reactions, several issues should be carefully dealt with. The inlet and outlet effect should be eliminated or accounted for Yue et al. (2007). Another important issue lies in the proper selection of material concentration to ensure that the operation condition along the microchannel fulfills the working criterion of the methods (i.e. fast reaction). The specific surface area of slug flow in microchannel includes the bubble lateral (film) and cap interfacial area. So to avoid the film saturation is of importance to obtain the actual surface area, because the film saturation would make the mass transfer through the lateral film inactive.

Fig. 16 shows the calculated specific surface area from captured images based on the assumed models. Under the experimental conditions, a varies from 3500 to 7200 m²/m³, which is within the range of data reported by Sobieszuk et al. (2011), Yue et al. (2007). As can be seen, a decreases with increasing liquid velocity or decreasing gas velocity. This is mainly due to the reduction of bubble length. The effect of gas velocity becomes less obviously above a certain value. As stated before, the increase in bubble size is slowed down when increasing gas velocity leads to a faster bubble generation process because of the inertia of forming bubble. Moreover, the film thickness also increases when inertia plays significant effect, making the bubble area decreases. The two effects hinder the specific surface area from further increasing at higher gas velocity.

4. Conclusions

This paper provides a glimpse into the behavior of gas–liquid slug flow under operating conditions where the flow rates are relatively high and inertial effects are non-negligible. Such information is important to understand the gas–liquid mass or heat transfer and reaction in microchannels, which are the basic for the use of microreaction technology in chemical industries.

The study has focused on the characteristics of slug flow with inertia effects in a rectangular microchannel with Y-junction. Visualization experiments using a high speed camera has been performed to study the frequency of gas bubble generation, the gas bubble and liquid slug lengths, the liquid film in the corners and at the lateral side walls, bubble velocities, the gas hold-up and specific surface area. This work highlights the inertia effect on the forming bubble during bubble formation under shearing regime.

Unlike the 'squeezing mechanism' with negligible inertia proposed by Garstecki et al. (2006), the main driving force for the pinch of the bubble thread is the liquid dynamic pressure and shearing stress exerted on the bubble, as well as the inertia of the emerging bubble. These factors result in increased frequency of bubble formation either when gas or liquid velocity increases. A revision of Garstecki model considering the inertia was proposed for the estimation of bubble length and shows relatively good agreement with experimental data. The new correlation allows a prediction of the gas bubble and liquid length under relatively large velocities, which is more common in the chemical industrial applications. The behavior of slug flow in rectangular channels must be different from that in circular channels since the corners significantly affect the whole flow behavior, especially in channels with large aspect ratio. Contrary to many researches, the slug length here decreases with increasing liquid velocity. This phenomenon together with the over prediction of bubble velocities from stagnant film hypothesis at high two-phase superficial velocities imply a strong leakage flow in the corners.

Based on the two dimensional image of bubbles, two simple models were assumed to calculate the film thickness in the corners, gas hold-up and specific surface area. Increasing gas velocity or liquid velocity would both lead to increase in the liquid film thickness. As described by Aussillous and Quéré (2000), Heil (2001), Kreutzer et al. (2005b), inertia has an effect on the film thickness. The thickening effect of inertia in this system was much stronger at high We that the thickening could be directly observed from the images. The void fracton and the gas hold-up under experimental conditions were found to follow the Armand-type correlation with the coefficient to be 0.914 and 0.899, respectively. The specific surface area shows a similar tendency to the gas bubble length, which increases with reducing liquid velocity or increasing gas velocity. However, the increase rate slows down at higher gas velocities.

Nomenclature

a	specific surface area, m^2/m^3
A	cross-sectional area, m^2
Ca	two phase capillary number defined by ($=\mu_L j_{TP}/\sigma_L$), dimensionless
D_H	Hydrodynamic diameter, μm
F	bubble frequency, Hz
J	superficial velocity, m/s
Q	flow rates, mL/min
U	velocity, m/s
W	channel width
We	two phase Weber number defined by ($=\rho_L u^2 D_H/\sigma_L$), dimensionless

Greek letters

α	void fraction, dimensionless
β	gas volumetric quality, dimensionless
δ	film thickness, μm
λ_1	constants in Eq. (1)
λ_2	constants in Eq. (1)
ε	gas hold-up, dimensionless

Subscripts

B	bubble
G	gas
L	liquid
S	slug
Mc	microchannel
TP	two phase

References

Abadie, T., Aubin, J., Legendre, D., Xuereb, C., 2012. Hydrodynamics of gas–liquid Taylor flow in rectangular microchannels. Microfluid. Nanofluid. 12, 355–369.

Abiev, R.S., 2008. Simulation of the slug flow of a gas–liquid system in capillaries. Theor. Found. Chem. Eng. 42, 105–117.

Akbar, M.K., Ghiaasiaan, S.M., 2006. Simulation of Taylor flow in capillaries based on the volume-of-fluid technique. Ind. Eng. Chem. Res. 45, 5396–5403.

Arias, S., Ruiz, X., Casademunt, J., Ramírez-Piscina, L., González-Cinca, R., 2009. Experimental study of a microchannel bubble injector for microgravity applications. Microgravity Sci. Technol. 21, 107–111.

Aussillous, P., Quéré, D., 2000. Quick deposition of a fluid on the wall of a tube. Phys. Fluids 12, 2367–2371.

Bretherton, F.P., 1961. The motion of long bubbles in tubes. J. Fluid Mech. 10, 166–188.

Choi, C.W., Yu, D.I., Kim, M.H., 2010. Adiabatic two-phase flow in rectangular microchannels with different aspect ratios: Part II—Bubble behaviors and pressure drop in single bubble. Int. J. Heat Mass Transfer 53, 5242–5249.

Choi, C.W., Yu, D.I., Kim, M.H., 2011. Adiabatic two-phase flow in rectangular microchannels with different aspect ratios: Part I—Flow pattern, pressure drop and void fraction. Int. J. Heat Mass Transfer 54, 616–624.

Chung, P.M.Y., Kawaji, M., 2004. The effect of channel diameter on adiabatic two-phase flow characteristics in microchannels. Int. J. Multiphase Flow 30, 735–761.

Fries, D.M., Trachsel, F., von Rohr, P.R., 2008. Segmented gas–liquid flow characterization in rectangular microchannels. Int. J. Multiphase Flow 34, 1108–1118.

Fu, T., Funfschilling, D., Ma, Y., Li, H.Z., 2009. Scaling the formation of slug bubbles in microfluidic flow-focusing devices. Microfluid. Nanofluid. 8, 467–475.

Günther, A., Khan, S.A., Thalmann, M., Trachsel, F., Jensen, K.F., 2004. Transport and reaction in microscale segmented gas–liquid flow. Miniatur. Chem. Biol. Bioeng. 4, 278–286.

Garstecki, P., Fuerstman, M.J., Stone, H.A., Whitesides, G.M., 2006. Formation of droplets and bubbles in a microfluidic T-junction-scaling and mechanism of break-up. Lab Chip 6, 437–446.

Guo, F., Chen, B., 2009. Numerical study on Taylor bubble formation in a microchannel T-junction using VOF method. Microgravity Sci. Technol. 21, 51–58.

Han, Y., Shikazono, N., 2009a. Measurement of liquid film thickness in micro square channel. Int. J. Multiphase Flow 35, 896–903.

Han, Y., Shikazono, N., 2009b. Measurement of the liquid film thickness in micro tube slug flow. Int. J. Heat Fluid Flow 30, 842–853.

Harris Wong, C.J.R., Morris, S., 1995. The motion of long bubbles in polygonal capillaries. Part 2. Drag, fluid pressure and fluid flow. J. Fluid Mech. 292, 95–100.

Hazel, A.L., Heil, M., 2002. The steady propagation of a semi-infinite bubble into a tube of elliptical or rectangular cross-section. J. Fluid Mech. 470, 91–114.

Heil, M., 2001. Finite Reynolds number effects in the Bretherton problem. Phys. Fluids 13, 2517.

Hui Liu, C.O.V., Rajamani, Krishna, 2005. Hydrodynamics of Taylor flow in vertical capillaries Flow regimes, bubble rise velocity, liquid slug length, and pressure drop. Ind. Eng. Chem. Res. 44, 4884–4897.

Ide, H., Kimura, R., Kawaji, M., 2007. Optical measurement of void fraction and bubble size distributions in a microchannel. Heat Transfer Eng. 28, 713–719.

Kawahara, A., Sadatomi, M., Nei, K., Matsuo, H., 2009. Experimental study on bubble velocity, void fraction and pressure drop for gas–liquid two-phase flow in a circular microchannel. Int. J. Heat Fluid Flow 30, 831–841.

Kawahara, A., Sadatomi, M., Nei, K., Matsuo, H., 2011. Characteristics of two-phase flows in a rectangular microchannel with a T-junction type gas–liquid mixer. Heat Transfer Eng. 32, 585–594.

Kawahara, A., Sadatomi, M., Okayama, K., Kawaji, M., Chung, P.M.Y., 2005. Effects of channel diameter and liquid properties on void fraction in adiabatic two-phase flow through microchannels. Heat Transfer Eng. 26 (13–19).

Kolb, W.B., Cerro, R.L., 1991. Coating the inside of a capillary of square cross-section. Chem. Eng. Sci. 46, 2181–2195.

Kolb, W.B., Cerro, R.L., 1993. The motion of long bubbles in tubes of square cross-section. Phys. Fluids A-Fluid Dyn. 5, 1549–1557.

Kreutzer, M.T., Kapteijn, F., Moulijn, J.A., Heiszwolf, J.J., 2005a. Multiphase monolith reactors: chemical reaction engineering of segmented flow in microchannels. Chem. Eng. Sci. 60, 5895–5916.

Kreutzer, M.T., Kapteijn, F., Moulijn, J.A., Kleijn, C.R., Heiszwolf, J.J., 2005b. Inertial and interfacial effects on pressure drop of Taylor flow in capillaries. AlChE J. 51, 2428–2440.

Kreutzer, M.T., van der Eijnden, M.G., Kapteijn, F., Moulijn, J.A., Heiszwolf, J.J., 2005c. The pressure drop experiment to determine slug lengths in multiphase monoliths. Catal. Today 105, 667–672.

Kuzmin, A., Januszewski, M., Eskin, D., Mostowfi, F., Derksen, J.J., 2011. Three-dimensional binary-liquid lattice Boltzmann simulation of microchannels with rectangular cross sections. Chem. Eng. J. 178, 306–316.

Laborie, S., Cabassud, C., Durand-Bourlier, L., Laine, J.M., 1999. Characterisation of gas–liquid two-phase flow inside capillaries. Chem. Eng. Sci. 54, 5723–5735.

Leclerc, A., Philippe, R., Houzelot, V., Schweich, D., de Bellefon, C., 2010. Gas–liquid Taylor flow in square micro-channels: new inlet geometries and interfacial area tuning. Chem. Eng. J. 165, 290–300.

Pohorecki, R., Kula, K., 2008. A simple mechanism of bubble and slug formation in Taylor flow in microchannels. Chem. Eng. Res. Des. 86, 997–1001.

Qian, D., Lawal, A., 2006. Numerical study on gas and liquid slugs for Taylor flow in a T-junction microchannel. Chem. Eng. Sci. 61, 7609–7625.

Saisorn, S., Wongwises, S., 2009. An experimental investigation of two-phase air–water flow through a horizontal circular micro-channel. Exp. Therm. Fluid Sci. 33, 306–315.

Saisorn, S., Wongwises, S., 2010. The effects of channel diameter on flow pattern, void fraction and pressure drop of two-phase air–water flow in circular micro-channels. Exp. Therm. Fluid Sci. 34, 454–462.

Saisorn, S., Wongwises, S., 2011. Two-phase air–water flow in micro-channels: an investigation of the viscosity models for pressure drop prediction. Int. Commun. Heat Mass Transfer 38, 212–217.

Sobieszuk, P., Cygański, P., Pohorecki, R., 2010. Bubble lengths in the gas–liquid Taylor flow in microchannels. Chem. Eng. Res. Des. 88, 263–269.

Sobieszuk, P., Pohorecki, R., Cygański, P., Grzelka, J., 2011. Determination of the interfacial area and mass transfer coefficients in the Taylor gas–liquid flow in a microchannel. Chem. Eng. Sci. 66, 6048–6056.

Taha, T., Cui, Z.F., 2004. Hydrodynamics of slug flow inside capillaries. Chem. Eng. Sci. 59, 1181–1190.

Thulasidas, T.C., Abraham, M.A., Cerro, R.L., 1995. Bubble-train flow in capillaries of circular and square cross-section. Chem. Eng. Sci. 50, 183–199.

Thulasidas, T.C., Abraham, M.A., Cerro, R.L., 1997. Flow patterns in liquid slugs during bubble-train flow inside capillaries. Chem. Eng. Sci. 52, 2947–2962.

Triplett, K.A., Ghiaasiaan, S.M., Abdel-Khalik, S.I., Sadowski, D.L., 1999. Gas–liquid two-phase flow in microchannels—Part I: Two-phase flow patterns. Int. J. Multiphase Flow 25, 377–394.

Völkel, N., 2009. Design and Characterization of Gas–Liquid Microreactors. Ph.D. Thesis. Institut of National Polytechnique de Toulouse, France.

van Baten, J.M., Krishna, R., 2004. CFD simulations of mass transfer from Taylor bubbles rising in circular capillaries. Chem. Eng. Sci. 59, 2535–2545.

van Steijn, V., Kleijn, C.R., Kreutzer, M.T., 2010. Predictive model for the size of bubbles and droplets created in microfluidic T-junctions. Lab Chip 10, 2513–2518.

van Steijn, V., Kreutzer, M.T., Kleijn, C.R., 2007. μ-PIV study of the formation of segmented flow in microfluidic T-junctions. Chem. Eng. Sci. 62, 7505–7514.

Vandu, C.O., Liu, H., Krishna, R., 2005. Mass transfer from Taylor bubbles rising in single capillaries. Chem. Eng. Sci. 60, 6430–6437.

Xiong, R., Chung, J.N., 2007. An experimental study of the size effect on adiabatic gas–liquid two-phase flow patterns and void fraction in microchannels. Phys. Fluids 19, 033301.

Yue, J., Chen, G., Yuan, Q., Luo, L., Gonthier, Y., 2007. Hydrodynamics and mass transfer characteristics in gas–liquid flow through a rectangular microchannel. Chem. Eng. Sci. 62, 2096–2108.

Yue, J., Luo, L., Gonthier, Y., Chen, G., Yuan, Q., 2008. An experimental investigation of gas–liquid two-phase flow in single microchannel contactors. Chem. Eng. Sci. 63, 4189–4202.

Yue, J., Luo, L., Gonthier, Y., Chen, G., Yuan, Q., 2009. An experimental study of air–water Taylor flow and mass transfer inside square microchannels. Chem. Eng. Sci. 64, 3697–3708.

Zhao, Y., Chen, G., Ye, C., Yuan, Q., 2013. Gas–liquid two-phase flow in microchannel at elevated pressure. Chem. Eng. Sci. 87, 122–132.